Fermi National Accelerator Laboratory

FERMILAB Pub-95/017-E
E665

Extraction of the Ratio F_2^n/F_2^p from Muon-Deuteron and Muon-Proton Scattering at Small x and Q^2

M.R. Adams et al.
The E665 Collaboration

Fermi National Accelerator Laboratory
P.O. Box 500, Batavia, Illinois 60510

February 1995

Submitted to *Physical Review Letters*

Operated by Universities Research Association Inc. under Contract No. DE-AC02-76CHO3000 with the United States Department of Energy

Disclaimer

Extraction of the ratio F_2^n/F_2^p from muon-deuteron and muon-proton scattering at small x and Q^2

M.R. Adams, [6] S. Aïd, [9] P.L. Anthony, [8] D.A. Averill, [6] M.D. Baker, [10] B.R. Baller, [4] A. Banerjee, [14] A.A. Bhatti, [15] U. Bratzler, [15] H.M. Braun, [16] T.J. Carroll, [11] H.L. Clark, [13] J.M. Conrad, [5] R. Davisson, [15] I. Derado, [11] S.K. Dhawan, [17] F.S. Dietrich, [8] W. Dougherty, [15] T. Dreyer, [1] V. Eckardt, [11] U. Ecker, [16] M. Erdmann, [1] G.Y. Fang, [5] J. Figiel, [7] R.W. Finlay, [13] H.J. Gebauer, [11] D.F. Geesaman, [2] K.A. Griffioen, [14] R.S. Guo, [6] J. Haas, [1] C. Halliwell, [6] D. Hantke, [11] K.H. Hicks, [13] V.W. Hughes, [17] H.E. Jackson, [2] D.E. Jaffe, [6] G. Jancso, [11] D.M. Jansen, [15] Z. Jin, [15] S. Kaufman, [2] R.D. Kennedy, [3] E.R. Kinney, [2] H.G.E. Kobrak, [3] A.V. Kotwal, [5] S. Kunori, [9] J.J. Lord, [15] H.J. Lubatti, [15] D. McLeod, [6] P. Madden, [3] S. Magill, [6] A. Manz, [11] H. Melanson, [4] D.G. Michael, [5] H.E. Montgomery, [4] J.G. Morfin, [4] R.B. Nickerson, [5] J. Novak, [12] S. O'Day, [9] K. Olkiewicz, [7] L. Osborne, [10] R. Otten, [16] V. Papavassiliou, [2] B. Pawlik, [7] F.M. Pipkin, [5,†] D.H. Potterveld, [2] E.J. Ramberg, [9] A. Röser, [16] J.J. Ryan, [10] C.W. Salgado, [4] A. Salvarani, [3] H. Schellman, [12] M. Schmitt, [5] N. Schmitz, [11] K.P. Schüler, [17] G. Siegert, [1] A. Skuja, [9] G.A. Snow, [9] S. Söldner-Rembold, [11] P. Spentzouris, [12] H.E. Stier, [1,†] P. Stopa, [7] R.A. Swanson, [3] H. Venkataramania, [17] M. Wilhelm, [1] Richard Wilson, [5] W. Wittek, [11] S.A. Wolbers, [4] A. Zghiche, [2] T. Zhao [15]

(Fermilab E665 Collaboration)

[1] *Albert-Ludwigs-Universität Freiburg i. Br., Germany*

[2] *Argonne National Laboratory , Argonne, Illinois 60439*

[3] *University of California, San Diego, California 92093*

[4] *Fermi National Accelerator Laboratory, Batavia, Illinois 60510*

[5] *Harvard University, Cambridge, Massachusetts 02138*

[6] *University of Illinois, Chicago, Illinois 60680*

[7] *Institute for Nuclear Physics, Krakow, Poland*

[8] *Lawrence Livermore National Laboratory, Livermore, California 94551*

[9] *University of Maryland, College Park, Maryland 20742*

[10] *Massachusetts Institute of Technology, Cambridge, Massachusetts 02139*

[11] *Max-Planck-Institut für Physik, Munich, Germany*

[12] *Northwestern University, Evanston, Illinois 60208*

[13] *Ohio University, Athens, Ohio 45701*

[14] *University of Pennsylvania, Philadelphia, Pennsylvania 19104*

[15] *University of Washington, Seattle, Washington 98195*

[16] *University of Wuppertal, Wuppertal, Germany*

[17] *Yale University, New Haven, Connecticut 06511*

† *Deceased.*

The ratio of the neutron to proton structure functions is measured at very small Bjorken x (down to 10^{-6}) and for $Q^2 > 0.001$ GeV^2 from scattering of 470 GeV muons on liquid hydrogen and deuterium targets. The ratio is found to be constant, at a value of $0.935 \pm 0.008 \pm 0.034$, for $x < 0.01$. This result suggests the presence of nuclear shadowing effects in the deuteron. The dependence of the ratio on Q^2 is also examined; no significant variation is found.

PACS numbers: 12.40.Vv,25.30.Rv,13.60.Le,24.85.+p

Submitted to Physical Review Letters

Jan 9, 1995

In the Parton Model the small–x behavior of the structure function ratio of neutrons to protons (F_2^n/F_2^p) in muon-nucleon scattering is related to the light–flavor sea–quark composition of the nucleon. Here $x = Q^2/2M\nu$ is the Bjorken scaling variable, where $-Q^2$ is the four-momentum transfer to the target nucleon squared, ν is the energy loss of the lepton in the laboratory frame, and M is the mass of the nucleon. From a different viewpoint, the small–x limit of muon-nucleon scattering coincides with the Regge limit for this process, and in this limit the ratio is expected to approach unity [1]. The most recent experimental test of the Gottfried sum rule [2] used a measurement of F_2^n/F_2^p and a fit to existing data for F_2^d, the deuteron structure function, with a result that indicated a flavor asymmetry of the light sea quarks [3]. The data cover $0.004 < x < 0.8$ and a Regge-inspired extrapolation is made to lower values of x. In addition, nuclear shadowing may be present at low x [4].

In this letter, we present a measurement of the structure–function ratio F_2^n/F_2^p in muon-nucleon scattering on hydrogen and deuterium targets [5]. The data cover the kinematic range $10^{-6} \leq x \leq 0.3$ and $10^{-3} \leq Q^2/\mathrm{GeV}^2$. The only previous data below x=0.004 are from an earlier measurement of this experiment [6]. The ratio F_2^n/F_2^p is equal to the single-photon-exchange cross section ratio of neutrons to protons if $R^n = R^p$, where R is the ratio of the total cross sections for longitudinally and transversely polarized virtual photons. This assumption is supported by the existing R measurements [7] which cover a portion of our kinematic range.

The data sample used in the present analysis was obtained during the 1991 Fermilab fixed-target run with the E665 apparatus [8], using muons of 470 GeV average energy. The apparatus consisted of a beam spectrometer used to measure the momentum of the incoming muons and a forward spectrometer that was used to reconstruct the final state of the interaction. The momentum resolution at 470 GeV was 0.4% for the beam and 1.0% for the forward spectrometer. Two targets, 0.99m long, of cryogenic liquid hydrogen (0.13 radiation lengths) and deuterium (0.15 radiation lengths) were used. An identical, evacuated, third target was used to correct for scatters that originated outside the target material. The three targets were cycled into the beam so that a different target was illuminated every machine cycle ($\sim$ 1 minute). This target cycling largely reduced time-dependent systematic effects in the ratio measurement. Essential for the small x measurement was the lead-gas electromagnetic calorimeter, 20 radiation lengths thick, which was located 25m downstream of the target. The calorimeter was fine-grained, with a transverse position resolution of 1 cm. Two different triggers were used to define the data sample for this analysis. The Small-Angle Trigger (SAT) [8] was a veto trigger that triggered on the absence of an unscattered muon at the expected position as defined by the incoming beam muon. The SAT allowed acceptance for muon scattering angles down to 0.5 mrad. The calorimeter (CAL) trigger accepted only

events with a large spatial spread of the energy deposited on the electromagnetic calorimeter [5], allowing acceptance down to the tracking resolution limit of Q^2 of 10^{-3} GeV^2.

Since acceptance and time-dependent efficiency effects largely cancel in the ratio measurement, the important experimental issues were to measure the relative normalization, understand the apparatus resolution effects, and remove the contribution of background processes. The main background comes from higher–order electromagnetic contributions to the total muon-nucleon inelastic cross section, and from muon-electron (μ–e) elastic scattering off the atomic electrons of the targets. The latter contribution is expected to appear as a peak centered at $x = m_e/M = 0.000545$, where m_e is the electron mass, with a width corresponding to the effects of the experimental resolution and radiative effects on the μ–e kinematics.

The flux of the incoming muons was obtained using randomly prescaled beam triggers. The beam trigger was defined by the presence of an incoming muon in the beam spectrometer. The beam trigger requirement was also part of the physics event trigger definition. The reconstruction efficiency and the phase–space cuts for the beams were taken into account in the normalization determination by imposing offline the same criteria for both beam and physics triggers. The prescale factor for the beam triggers was determined using two independent scaler systems, with excellent agreement ($\sim 0.02\%$) between the two measurements. The prescale factor, as well as the target pressure, was monitored every accelerator spill. To maintain the cancellation of time-dependent systematic effects, events were selected only from runs in which all targets were cycling into the beam and the target pressure was stable.

In order to minimize the effects due to experimental resolution and radiative background a series of selection criteria were applied. The beam and scattered muon tracks were required to be fully reconstructed and fitted to a vertex within the fiducial volume of the target, $\delta\nu/\nu < 0.3$, and $\delta x/x < 0.5$ (the latter only for the CAL trigger), where $\delta\nu$ and δx were the uncertainties in the measured ν and x. The kinematic range of the measurement was restricted to $0.1 < y < 0.8$, $\nu > 40$ GeV, $Q^2 > 0.1$ GeV^2 (0.001 GeV^2 for the CAL trigger), and $380 \leq E_{Beam} \leq 650$ GeV, where $y = \nu/E_{Beam}$ and E_{Beam} was the incident muon energy. After the beam phase-space selection the data sample consisted of 664 nb^{-1} of $\mu - p$ data and 749 nb^{-1} of $\mu - d$ data, which corresponded to $\sim$ 200,000 events per target.

The method most commonly used to extract the single-photon-exchange cross section from the total cross section, calculated radiative corrections [9], breaks down in the presence of background processes such as muon-electron elastic scattering. The event topology and information from the electromagnetic calorimeter were used to remove these events and those containing muon bremsstrahlung. Since the scattering angle for μ–e events (1 to 5 mrad) was small and all magnetic bends were in the horizontal plane, the scattered electron typically

deposited its energy within 10 cm of the center of the calorimeter in the vertical direction. The other major background, hard bremsstrahlung from the incoming or outgoing muon, shared a similar topology in the calorimeter. In this case the event signature was a high energy photon near the center of the calorimeter. In contrast, the muon-nucleon inelastic events deposited small–energy clusters over the entire calorimeter. A selection based on the energy of the largest-energy cluster in the calorimeter, normalized to the total available energy for the event (ν), and the calorimeter energy flow out of the horizontal plane [10,5] was used with the SAT data sample to remove the background events (electromagnetic rejection). The CAL trigger was designed to apply the same selection online as it triggered only on events with substantial energy out of the horizontal plane. The raw x distributions for the SAT data, with and without the electromagnetic (EM) rejection, and for the CAL data are shown in figure 1. The μ–e peak appears in the SAT sample with no EM rejection. The SAT sample after the EM rejection and the CAL trigger sample do not have any appreciable μ–e contribution.

A detailed Monte Carlo simulation, which included the effects of higher–order electromagnetic processes and muon-electron elastic collisions and which modeled secondary interactions and the response of the apparatus, was used to determine the performance of the EM rejection. It was found that this selection was fully efficient in removing μ–e elastic events, 98% efficient for bremsstrahlung events, and removed 7% of true inelastic events. These results are relevant in the region $x < 8 \times 10^{-4}$, where the effects of muon-electron scattering were significant. The CAL trigger was fully efficient in removing μ–e and hard bremsstrahlung events, but had a low acceptance for muon-nucleon inelastic events (30% at low x), since its response depended on the multiplicity of the event.

Based on the above background considerations, three different techniques have been developed to extract the ratio F_2^n/F_2^p from the measured event rates. In the region $x > 8 \times 10^{-4}$ which was unaffected by μ–e elastic scattering, the SAT data set was used with calculated radiative corrections [9]. The correction was applied as a weight on an event-by-event basis (the maximum correction on the ratio was $\sim 10\%$ at $x = 0.00092$ and $y = 0.8$). The second method used the SAT data set with the EM rejection and the third method the CAL data set. The ratio of the per nucleon structure function of the deuteron to that of the proton, F_2^d/F_2^p, is shown as a function of x in figure 2a) for the three different techniques. The ratio is extracted assuming $R^d = R^p$. In the region of overlap the three methods are in very good agreement. The curve shown is the prediction from [11], which includes nuclear shadowing

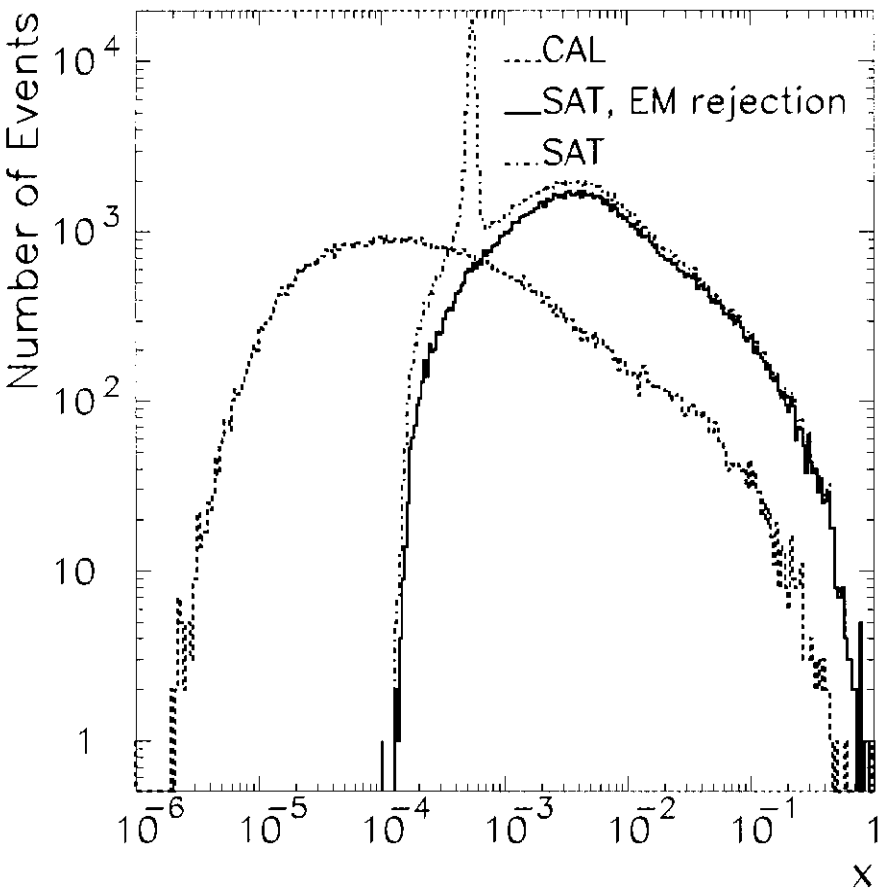

FIG. 1. The raw x distributions for hydrogen events, for the SAT trigger with and without the electromagnetic (EM) rejection and for the CAL trigger.

effects in the deuteron. In figure 2b) the ratio F_2^n/F_2^p, is shown as a function of x. In each bin the result from the technique with the smallest overall uncertainty is presented. The assumption in the extraction of F_2^n/F_2^p is that $F_2^d = \frac{1}{2}(F_2^n + F_2^p)$ (no nuclear effects in the deuteron.) The E665 results (solid symbols) are compared with the NMC results [3] (open symbols). The results from the two experiments are consistent. In table I F_2^n/F_2^p is given for each x bin, with the average Q^2 and the statistical and systematic uncertainty for each bin. The ratio is found to be significantly below unity for the entire kinematic range. The value obtained from a fit to a constant for $x \leq 0.01$ was 0.935 ± 0.008, (statistical uncertainty) and with $\chi^2/ndf = 12.41/15$.

The systematic uncertainty on F_2^n/F_2^p includes an x-independent component common to all methods, due to the cross–section normalization. This component has a 0.5% contribution from the relative beam normalization and a 0.85% contribution from the uncertainty in the target density and composition (the ratio is corrected for a small HD impurity in

the D_2 target). The SAT data with radiative corrections have a $\leq 2\%$ uncertainty due to overall acceptance differences and a $\leq 0.5\%$ uncertainty from the radiative correction procedure. The SAT data with EM rejection have the same acceptance uncertainty and a $\leq 0.6\%$ uncertainty due to the EM rejection. The CAL data have a $\leq 3.5\%$ uncertainty due to acceptance differences. The acceptance was determined using both the Monte Carlo simulation and monitoring triggers which were designed to study the response of the physics triggers. In the region where the CAL trigger did not overlap with other triggers, the hadronic final state properties on which the trigger probability depended were used to study the relative trigger acceptance [5].

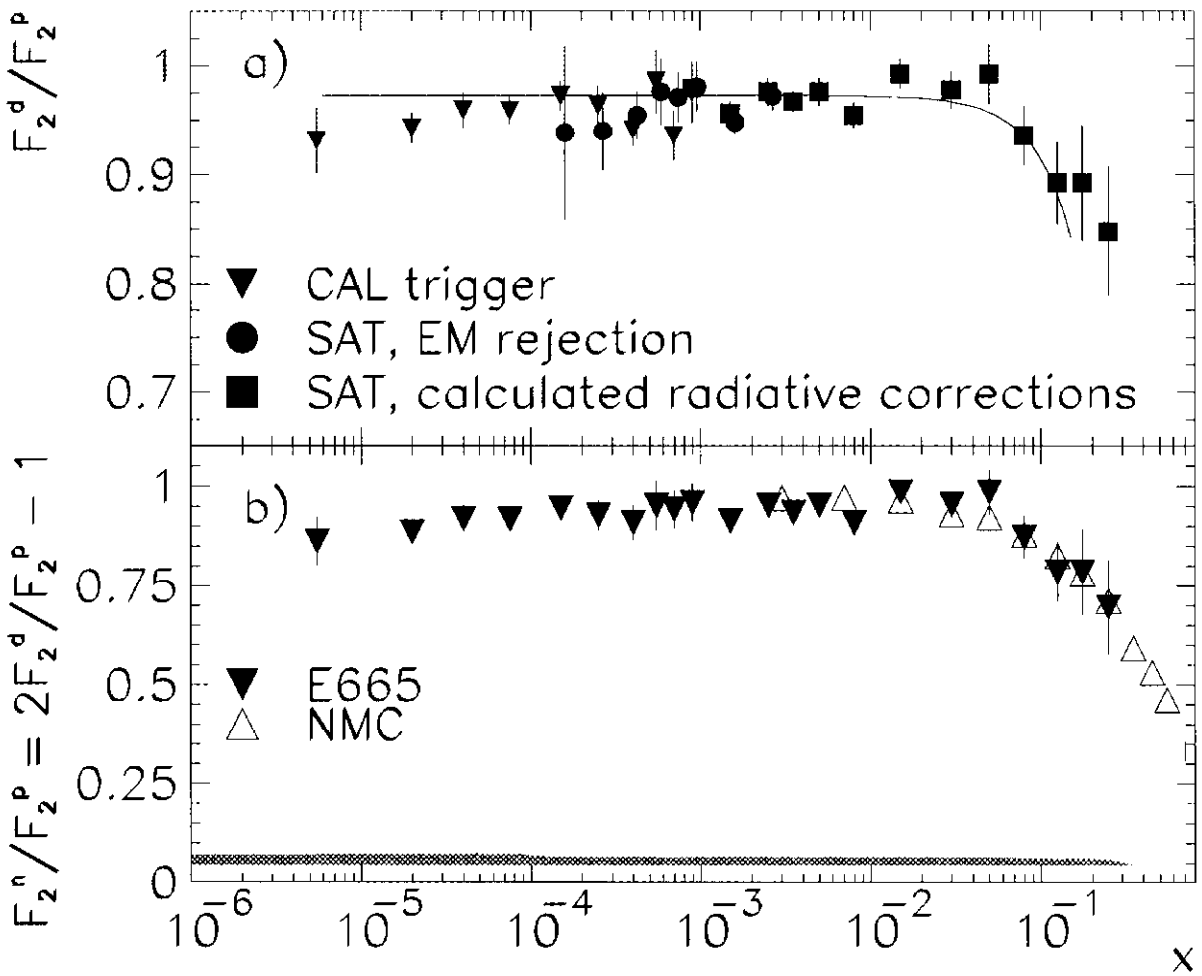

FIG. 2. a) F_2^d/F_2^p as a function of x, the curve shown is the prediction of [11]. b) $F_2^n/F_2^p = 2F_2^d/F_2^p - 1$ as a function of x, the NMC results from [3] are also shown. The hatched area represents the magnitude of the systematic uncertainty.

The muon-electron elastic scattering events provided a Monte Carlo-independent check of the relative normalization and calculated resolution. The muon-electron elastic peak from

each target was fitted to a gaussian for five Q^2 bins, and its mean was used to evaluate the electron mass ($m_e = Q^2/2\nu$). The values obtained from the two targets were in agreement within $1 \pm 0.5\%$, for all Q^2 bins. The muon-electron elastic–scattering cross–section ratio from the hydrogen and deuterium targets was measured to be 1.015 ± 0.020 (statistical uncertainty), which is consistent with the estimated normalization systematic uncertainty. The width of the peak is consistent with 5% resolution on the measurement of the x variable, in agreement with the Monte Carlo calculation. The absolute energy scale of the beam spectrometer has been obtained with accuracy of 0.26%, by measuring the momentum of

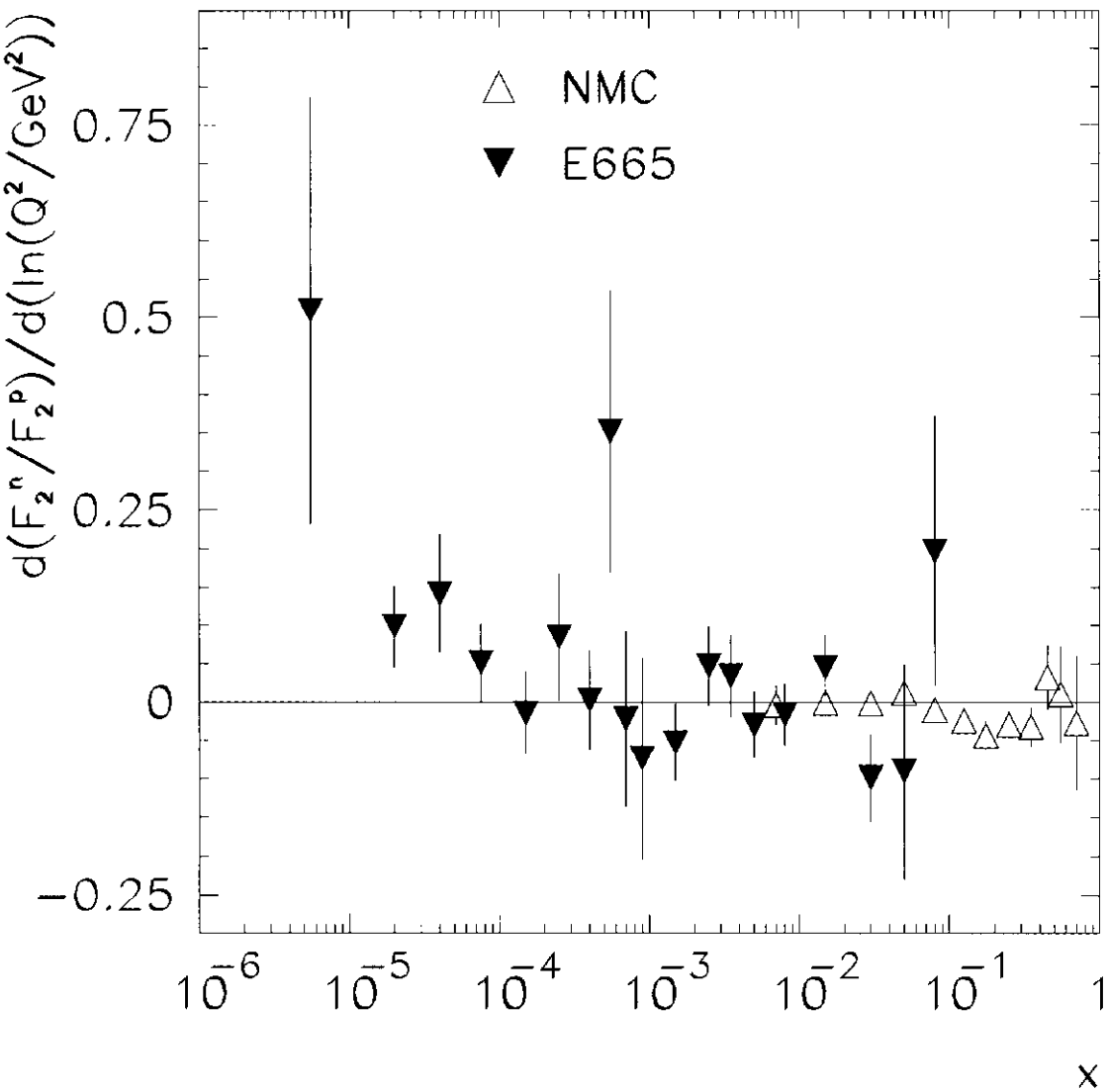

FIG. 3. Logarithmic Q^2 dependence of F_2^n/F_2^p as a function of x. The slope $d(F_2^n/F_2^p)/d(lnQ^2/GeV^2)$ is given at the center of each x bin. The NMC results from [12] are also shown.

primary protons from the Fermilab Tevatron. The relative energy scales of the beam and forward spectrometers agree within 0.5%, a result obtained by comparing the momentum measurement for unscattered beams from both spectrometers.

The logarithmic Q^2 dependence of the ratio was also examined. The Q^2 dependence of the ratio was parametrized in each x bin as a linear function of $\ln(Q^2/GeV^2)$. The logarithmic slopes as a function of x, compared with the NMC results from [12], are shown in figure 3 and listed in table I. There is no evidence for a significant Q^2 dependence of the ratio.

In summary, E665 has measured the structure function ratio $F_2^n/F_2^p = 2F_2^d/F_2^p - 1$ as a function of x and Q^2. The ratio as a function of x is below unity ($0.935 \pm 0.008 \pm 0.034$ for $x \leq 0.01$), a result that suggests the presence of nuclear shadowing effects in the deuteron. The magnitude of the observed effect is in agreement with model predictions [4]. The ratio does not show any significant Q^2 dependence as a function of x, also in agreement with model predictions [4].

We wish to thank all those personnel, both at Fermilab and at the participating institutions, who have contributed to the success of this experiment. This work was supported by the National Science Foundation, The U.S. Department of Energy, Nuclear Physics and High Energy Physics Divisions, the A.P. Sloan Foundation, the Bundesministerium für Forschung and Technologie and the Polish Committee for Scientific Research.

---

[1] B. Badełek, *et al.*, *Rev. Mod. Phys.* **64**, 927 (1992)

[2] K. Gottfried, *Phys. Rev. Lett.* **18**, 1174 (1967)

[3] M. Arneodo, *et al.*, *Phys. Rev.* **D50**, R1 (1994)

[4] B. Badełek, J. Kwieciński, *Nucl. Phys.* **B370**, 278 (1992); W. Melnitchouk, A.W. Thomas, *Phys. Rev.* **D47**, 3783 (1993)

[5] P. Spentzouris, *Ph.D. Thesis*, Northwestern U. (1994)

[6] M.R. Adams, *et al.*, *Phys. Lett.* **B309**, 477 (1993)

[7] P. Amaudruz, *et al.*, *Phys. Lett.* **B294**, 120 (1992); L. Whitlow , *et al.*, *Phys. Lett.* **B250**, 193 (1990)

[8] M.R. Adams, *et al.*, *Nucl. Inst. Methods* **A291**, 533 (1990)

[9] L.W. Mo and Y.S. Tsai, *Rev. Mod. Phys.* **41**, 205 (1969); The SLAC parametrization for R is used [7].

[10] M.R. Adams, *et al.*, *Phys. Rev. Lett.* **68**, 3266 (1992)

[11] B. Badełek and J. Kwieciński, *Phys.Rev.* **D50**, R4 (1994)

[12] P. Amaudruz, *et al.*, *Nucl. Phys.* **B371**, 3 (1992)

TABLE I. $F_2^n/F_2^p = 2F_2^d/F_2^p - 1$ as a function of x. For each bin, the result from the method with the smallest overall uncertainty is given. The systematic uncertainty on the Q^2 dependence is negligible as compared to the statistical uncertainty.

x bin	$< Q^2 >$ GeV^2	F_2^n/F_2^p ±statistical ±systematic error	$\frac{d(F_2^n/F_2^p)}{d(lnQ^2/GeV^2)}$ ± statistical error
0.000001-0.00001	0.002	0.862±0.061±0.027	0.508±0.274
0.000010-0.00003	0.005	0.886±0.027±0.028	0.098±0.052
0.000030-0.00005	0.011	0.919±0.033±0.029	0.141±0.076
0.000050-0.00010	0.022	0.918±0.026±0.029	0.051±0.050
0.000100-0.00020	0.043	0.944±0.027±0.030	-0.014±0.053
0.000200-0.00030	0.072	0.927±0.036±0.029	0.085±0.082
0.000300-0.00050	0.201	0.909±0.044±0.021	0.002±0.063
0.000500-0.00060	0.252	0.952±0.061±0.022	0.352±0.183
0.000600-0.00079	0.293	0.943±0.045±0.022	-0.022±0.112
0.000790-0.00100	0.344	0.959±0.045±0.021	-0.074±0.130
0.001000-0.00200	0.437	0.913±0.022±0.020	-0.052±0.049
0.002000-0.00300	0.561	0.952±0.027±0.021	0.046±0.051
0.003000-0.00400	0.668	0.934±0.029±0.021	0.034±0.052
0.004000-0.00600	0.857	0.952±0.025±0.021	-0.029±0.042
0.006000-0.01000	1.277	0.909±0.024±0.020	-0.015±0.039
0.010000-0.02000	2.383	0.986±0.027±0.022	0.045±0.043
0.020000-0.04000	4.928	0.955±0.033±0.021	-0.098±0.056
0.040000-0.06000	8.125	0.985±0.054±0.022	-0.090±0.138
0.060000-0.10000	12.219	0.872±0.055±0.019	0.196±0.175
0.100000-0.15000	18.634	0.785±0.074±0.017	
0.150000-0.20000	24.143	0.784±0.107±0.017	
0.200000-0.30000	35.588	0.700±0.119±0.016	